Stabilizing Iodine in 2D Mixed Halide Perovskites: Dion–Jacobson versus Ruddlesden–Popper Phases

Junsang Cho[1*], Manish Mukherjee[2,3], Gábor Szabó[2,3], Seonhong Min[1], and Prashant V. Kamat[2,3,4*]

[1]School of Energy and Chemistry, Sungshin Women's University, Seoul 01133, South Korea

[2]Notre Dame Radiation Laboratory, [3]Department of Chemistry and Biochemistry, and

[4]Department of Chemical and Biomolecular Engineering, University of Notre Dame, Notre Dame, Indiana 46556, United States

Corresponding Authors: jcho3@sungshin.ac.kr**;** pkamat@nd.edu**;**

Abstract

Iodine electrochemistry plays a critical role in driving iodide-oxidation induced halide migration in 3D halide perovskites. When subjected to light illumination or electrochemical bias, mixed halide perovskites undergo halide segregation followed by iodine expulsion from the crystal lattices. To mitigate such intrinsic halide ion mobility in 3D perovskites, lower-dimensional (2D) perovskites are employed as barriers to stabilize the perovskite layers. Interestingly, 2D halide perovskites also exhibit halide ion mobility that is dependent on the binding configuration viz., Ruddlesden–Popper (RP) and Dion–Jacobson (DJ) perovskites. Hybrid RP-DJ perovskites with a mixed Br:I ratio of 50:50 show increased stability following a continuous photoirradiation. Spectroscopic studies that probe iodine migration and expulsion in photoirradiated 2D films of different configurations are presented here. The effective strategy of blending two different 2D phases (RP-DJ) offers new opportunities to develop stable 2D/3D perovskite interfaces in solar cells

For Table of Contents Use Only

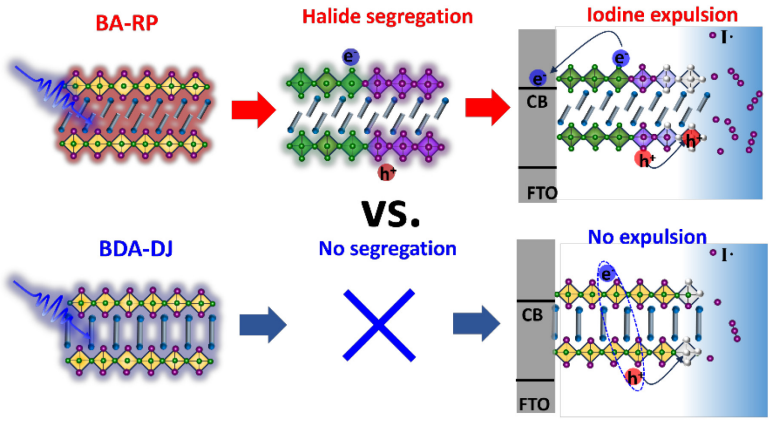

Introduction

Halide ion migration in halide perovskites remains a significant hurdle in developing stable perovskite optoelectronics and further commercialization.[1–4] Under photoirradiation and electrochemical bias, 3D halide perovskites undergo defect-mediated halide ion migration. One interesting aspect of halide ion migration is the photoinduced phase segregation in the mixed halide perovskites leading to the formation of Br- and I-rich domains.[5–9] Accumulation of holes at iodide (I^-) sites has been shown to facilitate iodide oxidation to form iodine ($I\cdot$) interstitial and iodide vacancies (I_V^+), leading to iodide migration through these defect sites.[3,10,11] Although such halide segregation is mostly reversible upon removal of short term illumination, continuous illumination can accumulate holes and drive expulsion of iodine from crystal lattice.[10–14] As such, these sequential processes (viz., hole trapping, oxidation and expulsion of iodine) collectively accelerate the degradation of perovskite device performance during operation.[15,16]

To mitigate such instability issues of 3D halide perovskites, lower-dimensional 2D perovskites with layered structures have been developed to create two-dimensional (2D)/three-dimensional (3D) bilayer heterostructures or quasi-2D frameworks.[17–20] Compared to conventional 3D counterparts, the reduced dimensionality of these layered structures is effective in suppressing halide ion migration.[9,21–24] While the intercalated spacer cations in 2D perovskites have negligible impact on the optoelectronic properties of 2D/3D architectures (e.g., bandgap), their chemical structure offers different degree of stability. Specifically, the molecular descriptors of spacers including molecular weight, aromaticity, glass transition temperature, surface dipole moment introduced by heteroatom (S or F), and binding configuration motifs, etc. play a crucial role in determining ion transport and structural stability.[25–28] Based upon binding configuration of spacer cations, these 2D perovskites are further classified into two subgroups: 1) Ruddlesden–Popper (RP) phase and 2) Dion–Jacobson (DJ) phase.[29–31] The former is reliant on van der Waals interactions of monodentate spacer cations such as butylammonium (BA^+) whereas the latter is constructed with covalent interlayer linkage of bidentate spacers such as 1,4-butylenediamine (BDA^{2+}).

An overlooked fact in designing 2D/3D perovskite interfaces is the ease with which both cations and anions (halides) migrate under photoirradiation. For example, under continuous photoirradiation or thermal stress, 2D/3D interfaces drives the spacer cation exchange reaction due to entropic-driven mixing.[32–36] Such spacer cation exchanges proceeds more readily in soft RP perovskites than in rigid DJ counterparts.[32,33,37]. Covalently tethered DJ phases strengthen whole 2D lattice frameworks, thus maintaining the 2D lattice frameworks under external stimulus.[27,38–41] Such molecular reinforcement strategy is oftentimes employed in rigidifying the entire perovskite frameworks and suppressing a defect-mediated halide ion migration.[24,42,43] Recent studies have shown that synergetic incorporation of both RP-DJ spacer cations can improve vertical orientation, narrow phase distribution, and device performance under thermal and humidity stress in quasi-2D perovskites.[30,44–46] However, such mechanistic understanding beyond 2D spacer hybrid engineering yet remains limited, particularly regarding how each phase influence stability of the mixed halide phases.

We have now investigated how the binding configuration of spacer cations in 2D mixed halide perovskites with a Br:I ratio of 50:50 influences the iodine stability. Under continuous photoirradiation, these 2D perovskites, when in contact with a solvents such as dichloromethane (DCM) or dichloroethane (DCE), undergo halide segregation followed by iodide expulsion into the solvent.[23,24,47] By tracking the spectral changes, we can understand the kinetics of both segregation and expulsion of iodine species from 2D perovskite lattices. Absence of halide segregation in DJ phase prevent hole transfer and accumulation at I-rich domain, thus suppressing iodide expulsion and degradation of the mixed halide phase (and simultaneously inducing electron-hole recombination within mixed halide phases).[7,13–15,48] Spectroscopic and structural analyses of different phase compositions of 2D mixed halide perovskites (RP:DJ = 100:0 – 0:100) presented in this study provide new insights into the role of spacer cations in dictating overall photostability. These results, which provide fundamental insights into the design principles of phase-stable 2D perovskites, offer new strategy for developing stable wide-bandgap perovskite optoelectronic applications.

Results and Discussion

Photoinduced Segregation and Expulsion in 2D Perovskites. The spacer cations employed in 2D perovskites dictate rigidity of 2D perovskite frameworks, quantum and dielectric confinements, interfacial energetics, and structural stability.[49,50] To investigate the effect of spacer binding motifs

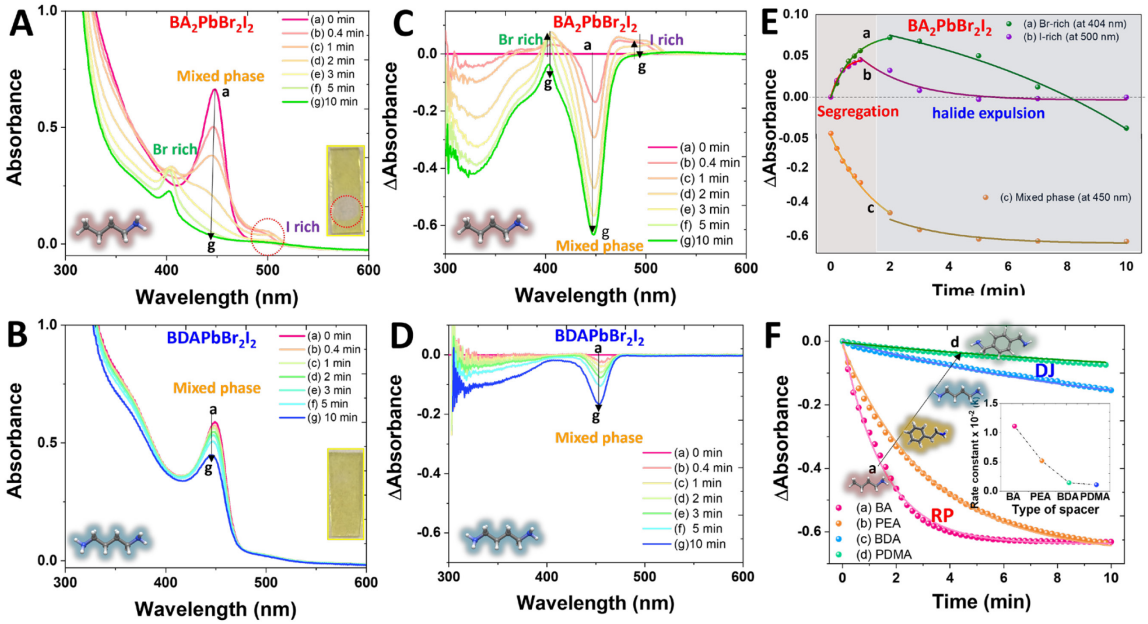

Figure 1. (A,B) Absorption (C,D) difference absorption spectra of (A,C) $BA_2PbBr_2I_2$ (RP-BA 100%) and (B,D) $BDAPbBr_2I_2$ (DJ-BDA 100%) under 405 nm diode laser irradiation with light intensity of 25 mW/cm^2. Insets of 1A,B show the digital photographs taken after 10 min irradiation of 405 nm diode laser. (E) Corresponding kinetic traces and monoexponential fits for halide ion segregation followed by expulsion. (F) Kinetic traces and fitting by tracking the mixed halide phase peak at 450 nm of 2D perovskites with a ratio of Br:I = 50:50 using different spacer ligands during a 405 nm laser diode irradiation with light intensity of 25 mW/cm^2.

on the mixed halide stability in 2D perovskites, we prepared 2D perovskite films with the same halide composition of Br:I =50:50, based on different binding configurations of BA-RP and BDA-DJ (see Experimental for details). Note that the spacer cations of BA and BDA have the same carbon chain length (C4) with only different numbers of ammonium groups. Upon substitution of Br with I, both BA-RP and BDA-DJ perovskite films exhibit similar halide-dependent bandgap changes from 2.4(2.5) – 3.1 (3.2) eV (**Figure S1**).

As-prepared 2D mixed halide perovskite films, $BA_2PbBr_2I_2$ (RP) and $BDAPbBr_2I_2$ (DJ), exhibit pronounced band-edge absorption peaks at wavelengths of 445 and 450 nm respectively (**Figures 1A,B**). When subjected to a continuous wave (CW) 405 nm laser diode irradiation of 2D perovskite film in contact with dichloroethane (DCE) solvent, they exhibit different photoinduced behaviors (**Figures 1A,B)**. For BA-RP-perovskites, the band-edge absorption continuously decreased from 0.8 to nearly 0 over 10 min irradiation, (**Figure 1A**). The difference absorption spectra (**Figures 1C,D**) further corroborates that BDA-DJ based 2D perovskites show enhanced stability compared to BA analogues. During early period of first 2-3 min, new absorption bands arise at 400 nm and 500 nm, corresponding to Br-rich (~ 400 nm) and I-rich (~ 500 nm) domains (**Figure 1B**). These absorption features correspond to halide segregation at early times. In contrast, the BDA-DJ perovskites displayed relatively small changes at band-edge absorption of 450 nm (**Figure 1D**). Digital photographs taken after photoirradiation as shown in insets of Figures 1A,B show the robustness of DJ perovskite films compared to RP counterparts. The photoinduced transformations in these 2D perovskites are described in the following equations (1-3) using $BA_2PbBr_2I_2$ as an example (**Scheme 1**).

$$\text{Photosegregation: } 2BA_2PbBr_2I_2\ (h\nu) \rightarrow\ BA_2PbBr_4 + BA_2PbI_4 \qquad (1)$$

$$\text{Hole trapping and oxidation: } BA_2PbI_4 + 2h^+ \rightarrow PbI_2 + 2BA^+ + I_2 \qquad (2)$$

$$\text{Dissolution: } BA_2PbI_4 \rightarrow PbI_2 + 2BA^+ + 2I^- \qquad (3)$$

By tracking temporal evolution of absorption changes at 404, 450 and 500 nm, one can elucidate the kinetics of halide ion segregation as well as iodine expulsion (**Figure 1E**). Initially,

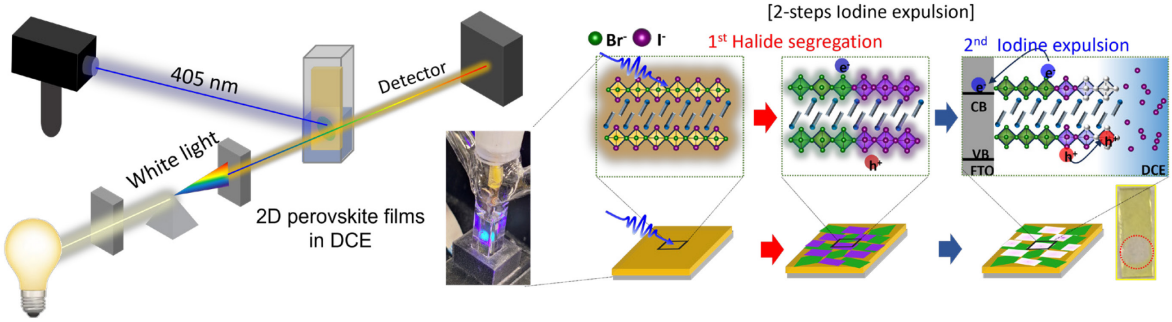

Scheme 1. Schematic illustration of photoinduced iodide expulsion and iodine expulsion mechanism seen in $BA_2PbBr_2I_2$ (BA 100%) film emersed in DCE solvent, including two steps (halide segregation followed by iodide expulsion).

photosegregation of the mixed halide film is driven by the cascade of charge transfer and hole accumulation at I-rich sites of the lower bandgap semiconductor.[3,16,47] Since the oxidation potential of Br^-/Br_2 is greater (E^0 = +1.08 V vs. NHE) compared to I^-/I_2 (E^0 = +0.62 V vs. NHE) the bromide species are not readily oxidized (**Figure 1E**). Again, these observations suggest that BDA-DJ perovskite films possess rigidized 2D frameworks with covalent interlayer linkage of spacer cations.

To further validate our observation that DJ structures offer better photostability than RP structures under photoirradiation, we repeated the experiments with two additional spacer cations, viz., phenethylamine (PEA) and 1,4-phenylenedimethylamine (PDMA). The changes in the absorption spectra under photoirradiation are included in **Figure S2**. As can be monitored at band-edge absorption peak of 440-450 nm, the kinetic traces with four different spacers (BA, PEA, BDA, and PDMA) are compared in **Figure 1F**. The pseudo-first order rate constant ($k_{segregation}$), corresponding to the disappearance of mixed halide composition, decreased from 1.1×10^{-2} sec^{-1} (BA-RP) to 1.2×10^{-3} sec^{-1} (PDMA-DJ) by an order of magnitude. Although PEA-based mixed halide perovskites are often reported as relatively resistant to photoinduced halide segregation,[51–53] we observed significantly accelerated photosegregation. The previous studies with PEA spacer cations were typically performed on solvent-free dry film, wherein the halide ion mixing can occur reversible within the crystal lattices even under photoirradiation.[51–53] However, under our experimental conditions with DCE solvent, the forward process is accelerated through a two-step pathway (**Scheme 1**) including the initial mixed halide segregation followed by irreversible iodine expulsion into solvent. Generally, our recent studies have established the combined effects of binding configurations (RP vs DJ) and van der Waals interactions (linear vs aromatic) in these spacer cations. The binding configuration alteration between RP and DJ with the same carbon chain of spacer cations is the most effective strategy by suppressing such photoinduced segregation.[51,52,54] By employing the DJ spacer ligands, either BDA or PDMA, we can suppress halide segregation and subsequent halide expulsion, consistent with earlier reports.[25,52,55] The tightly bound DJ architecture slows the halide ion migration. In addition to binding motif, introduction of aromatic ligands in spacer ligand molecules may also enhance the stability by adding extra van der Waals interactions through π-π stacking of phenyl rings.[56–59]

Construction of RP-DJ Hybrid Perovskites. Even though DJ spacers provide greater stability than RP counterparts, many perovskite optoelectronics still rely on the RP spacer cations due mainly to facile processing conditions with increased solubility.[19,27,41] Therefore, a strategy to mitigate the intrinsic limitation of volatile RP spacers prompted us to examine systematic blending of BA and BDA spacer cations in 2D perovskite films. This approach allowed us to synergistically enhance stability of hybrid RP-DJ phase compositions. Mixed RP-DJ perovskite films were fabricated through stoichiometric blending of BA-RP (n = 1) and BDA-DJ (n = 1) perovskites in the precursor solution. By varying the volumetric ratio of RP:DJ from 100:0 (pure BA) to 0:100 (pure BDA) we were able to compose five different compositions in the film. Corresponding crystal structure changes with varying the RP-DJ phase composition were investigated by X-ray

diffraction (XRD) as shown in **Figures 2A,B**. Note that unlike the 3D mixed perovskites wherein the halides are homogeneously distributed at the unit cell level, the 2D mixed halides exhibit preferential occupation of Br and I due to different ionic radii. The larger I^- (216 pm) preferentially occupies the apical position while the smaller Br- reside (195pm) along equatorial sides.[60] The recorded XRD patterns show periodic repeating along (00l) planes of pure 2D perovskites with 100% BA and 100% BDA, determining interlayer spacing of 1.4 nm (BA) and 1.0 nm (BDA) (**Figures 2B and S3**).[21,54,61] At the mixed RP-DJ composition of 50:50, decreasing the portion of BA fraction or increasing the BDA fraction led to disappearance of BA phase at 6.4° (002 plane) and concurrent appearance of BDA analogues at 8.2° (002 plane) (**Figure 2B**). These results reflect that the BA and BDA spacers form separate crystallographic domains while maintaining own interlayer spacing distances (**Figure 2A**).[25,62]

The binding energies of Pb-X bonds were further investigated for the mixed RP:DJ perovskites using X-ray photoelectron spectroscopy (XPS), further supporting the distinctive crystallographic domain formation in BA-RP and BDA-DJ films (**Figure 2C**). The binding energy of Pb $4f_{7/2}$

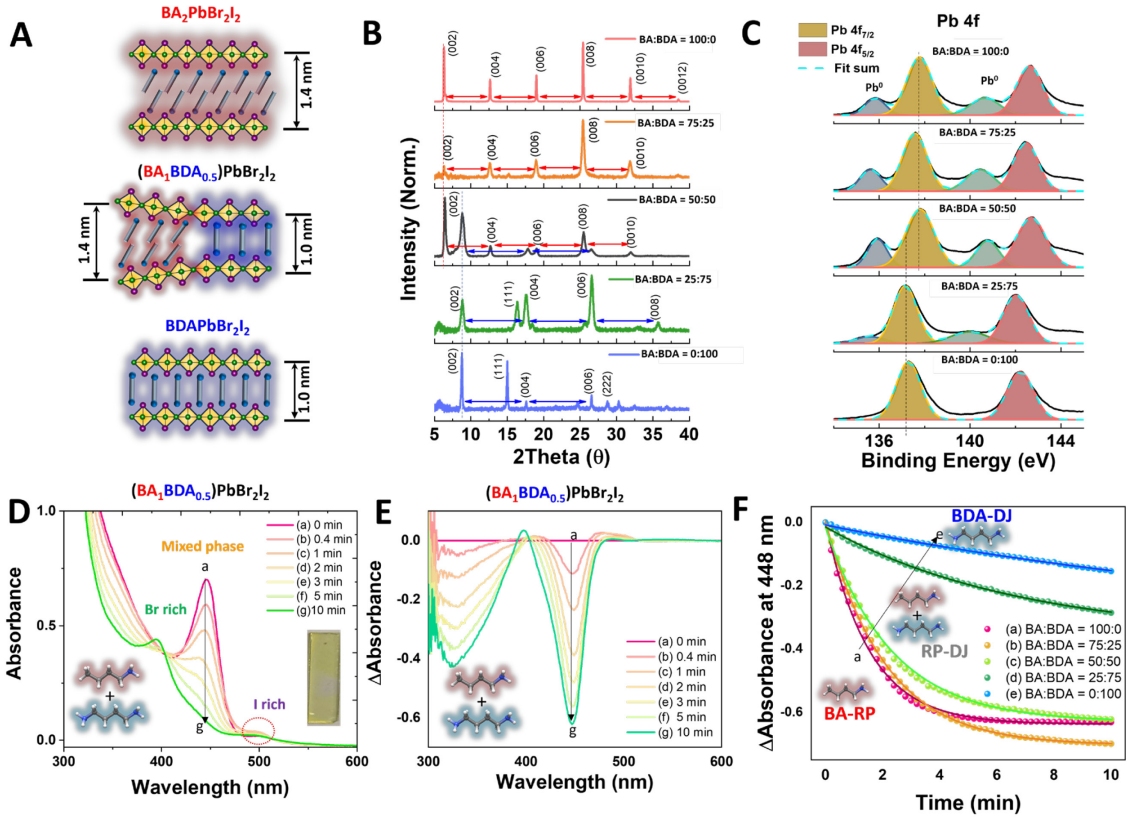

Figure 2. (A) Schematic illustration of crystal structure changes in mixed RP:DJ hybrid compositions. (B,C) Evolution of XRD patten (B) and XPS (C) with varying the ratio of $BA_2PbBr_2I_2$ and $BDAPbBr_2I_2$ perovskites ranging from BA:BDA = 100:0 to 0:100. (D,E) Absorption (D) and difference absorption (E) spectra recorded for $BA_1BDA_{0.5}PbBr_2I_2$ perovskites (BA:BDA = 50:50) during CW 405 nm diode laser irradiation with intensity of 25 mW/cm^2. (F) Kinetic traces and fitting at tracking the mixed halide phase (at 440-450 nm) for mixed RP-DJ perovskites.

observed in 2D perovskite films was determined to be 137.8 (pure BA) and 137.3 eV (pure BDA), indicative of decreased binding energy in DJ perovskites with -0.5 eV relative to RP ones (**Figure 2C**). The decreased binding energy of Pb 4f atom is associated with incorporation of divalent BDA^{2+}, withdrawing the electron density over Pb-X bonds (X= Br and I). Therefore, the same trend of binding energy shift in I 3d and Br 3d were observed for BA-RP and BDA-DJ films. Once again, these results corroborate the tighter binding nature of DJ perovskites **(Figure S4 and Table S1**). In the case of mixed RP-DJ hybrid, two different domain peaks of Pb $4f_{7/2}$ spectra were found (**Figure 2C**). For BA:BDA = 50:50, the broadened XPS spectra of $Pb_{7/2}$ and $Pb_{5/2}$ seen in this sample were spectrally deconvoluted to assign each contribution from BA and BDA perovskites, confirming similar contribution from BA (36-45 %) and BDA (55-64 %) (**Figure S5**). Additionally, the formation of Pb^0 also significantly decreased in DJ perovskites, suggesting another evidence of stabilizing the Pb-X bonds.[63,64]

Additionally, the photoluminescence (PL) emission and infrared (IR) vibrational analyses were carried out to elucidate the structural transformation in these hybrid RP-DJ perovskite films (**Figure S6**). The PL emission of $BA_2PbBr_2I_2$ film exhibits two pronounced emissions centered at 470 nm and 510 nm. The longer-wavelength emission is attributed to segregated I-rich domain upon the measurement of PL emission spectra under white light illumination, consistent with earlier report.[52] Upon increasing the fraction of BDA-DJ, overall PL emission progressively decreased and quenched. The suppressed PL emission intensity observed in DJ-rich composition arises from more dominant nonradiative recombination that resulted from stronger interlayer electronic coupling and reduced exciton confinement, in good agreement with earlier report.[65] Consistent trends are observed in the IR spectra, which display a systematic increase in the intensity of the $–NH_3^+$ stretching vibrations with increasing BDA content. This behavior reflects the incorporation of the diammonium spacer, where the dual ammonium in BDA amplifies hydrogen-bonding interactions with the inorganic framework, thereby strengthening the corresponding vibrational modes.

The photoirradiation experiments were repeated with mixed RP-DJ films with phase compositions of RP:DJ ratio of 75:25, 50:50, and 25:75, respectively (**Figure S7**). The representative examples of absorption and difference absorption spectra recorded with RP:DJ = 50:50 during photoirradiation are shown in **Figures 2D,E**. The absorption corresponding to excitonic band decreased with continued irradiation using CW 405 nm diode laser. Interestingly, the formation of segregated halide phases at 400 (Br-rich) and 500 nm (I-rich) was significantly suppressed compared to BA-RP (100% BA) perovskite film. These observations were corroborated by digital photograph taken after 10 minutes of photoirradiation (Insets of **Figure 2D**). **Figure 2F** compares the absorption decay and monoexponential kinetic fits recorded for different RP:DJ compositions by tracking the mixed halide compositions at 440-450 nm for all five mixed RP-DJ hybrids. The pseudo-first order rate constants ($k_{segregation}$) decreased from 1.1×10^{-2} sec^{-1} for BA-RP (100% BA) to 1.4×10^{-3} for BDA-DJ (100% BDA) perovskite films. The dependence of rate constant on the fraction of BDA in the RP-DJ hybrid perovskite film is shown in **Figure S8**. As the fraction of DJ

perovskites within the mixed RP-DJ hybrid is increased, 2D frameworks become more rigidized, resulting in the suppression of the halide ion migration. This rigidification achieved through the introduction of DJ-phase in the RP:DJ hybrid film in turn makes the photo segregation and halide expulsion less favorable.[66]

An attempt was made to visualize morphological changes that occur during photoirradiation of three representative films, $BA_2PbBr_2I_2$, $BA_1BDA_{0.5}PbBr_2I_2$, and $BDAPbBr_2I_2$, using scanning electron microscopy (SEM). The SEM images of these three films with RP-DJ phase compositions of RP:DJ ratio, 100:0, 50:50, and 0:100 are shown in **Figure 3**. For pristine 2D perovskite films with 100% BA and 100% BDA, the average grain sizes were determined to be 70 ± 20 nm and 210 ± 40 nm respectively. The mixed RP-DJ films, however, show two different sizes of crystallographic domains as indicated by red (BA-RP) and yellow circles (BDA-DJ) in SEM images (**Figures 3A-C**). It is worth mentioning that during nucleation and growth stage of spin-coating, we observed slower color change in BDA-DJ films as compared to BA-RP counterparts suggesting difference in the crystallization process of the two films. Such slowed kinetics is expected to promote the larger grain size in BDA-DJ films. The difference in binding ability of monodentate BA and bidentate BDA spacer cations to Pb^{2+} monomer in the precursor solution is likely to influence nucleation and growth kinetics of RP and DJ perovskite phases. SEM images of these films recorded after 405 nm irradiation (25 mW/cm^2) for 10 minutes are shown in **Figures 3D-F**. SEM images taken for BA-RP perovskite film revealed the creation of numerous pinholes and defects due to photoinduced halide expulsions (**Figure 3D**). In contrast, the mixed RP-DJ perovskites with a BA:BDA ratio of 50:50 (**Figure 3E**) and BDA-DJ films (**Figure 3F**) exhibit significantly reduced pinhole formation compared to BA-RP perovskite films. These observations

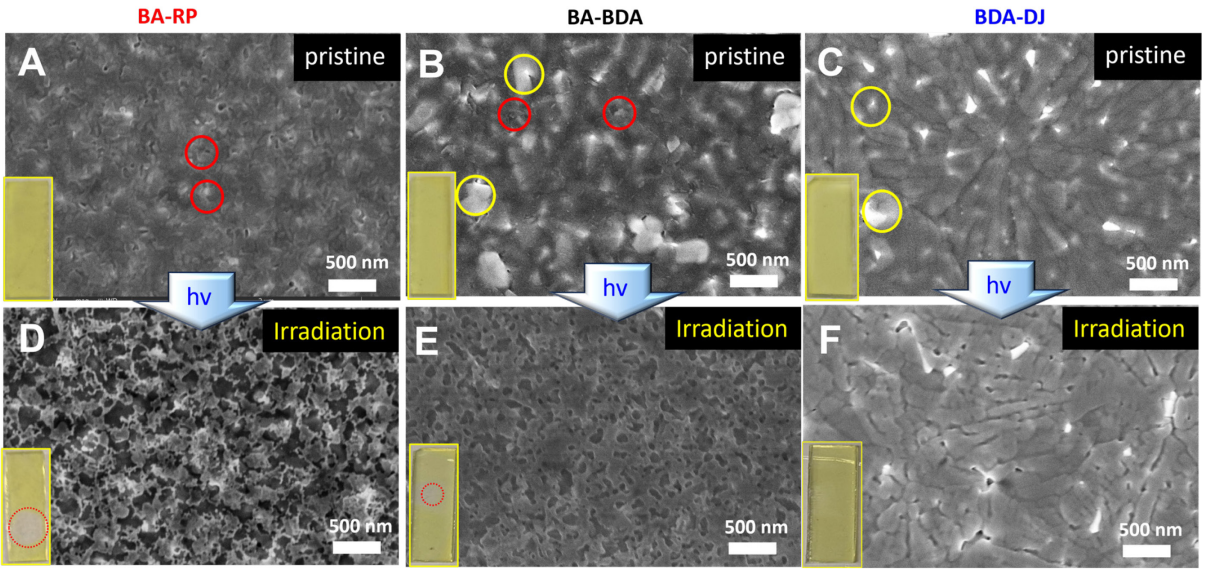

Figure 3. (A-F) SEM images of (A,D) $BA_2PbBr_2I_2$ (pure BA 100%), (B,E) $BA_1BDA_{0.5}PbBr_2I_2$ (BA:BDA =50:50), and (C,F) $BDAPbBr_2I_2$ (pure BDA 100%), respectively, before (A-C) and after (D-F) a CW 405 nm diode laser irradiation for 10 min. Inset of each panel display the digital photograph of these films taken after 10 minute irradiation.

are consistent with the degradation trend seen in spectroscopic observations (**Figure 1**). As discussed in the previous section, XRD and XPS studies of mixed crystallographic domains with RP-DJ phases decreased the susceptibility to photoinduced iodide expulsion.

Excited State Charge Carrier Dynamics. To further elucidate the primary photochemical events leading to iodine migration and expulsion, we probed the excited-state charge dynamics of 2D mixed halide perovskite films using ultrafast pump-probe spectroscopy. Transient absorption (TA) spectra were recorded using the excitation at 400 nm pump laser (fluence of 32 μJ/cm^2) and probe delay times of 1-700 ps (**Figures 4A-C**). For probing the excited-state events during the halide segregation, the 2D perovskites films were continuously irradiated with a CW 405 nm diode laser with intensity of 50 mW/cm^2 (see insets of **Figures 4B,C**). It should be noted that the pulsed laser excitation does not bring about halide phase segregation.

The TA spectra recorded with BA-RP perovskite film without continuous irradiation in shown in **Figure 4A**. The TA spectra of partially (5 min irradiation) and fully segregated (10 min irradiation) BA-RP films are shown in **Figures 4B,C.** The pristine BA film was characterized by single ground state bleach at 460 nm representing depopulation of the excitonic band as excited with pump-excitation (**Figure 4A**). For the segregated films after a 405 nm laser irradiation of 5 minutes, an additional bleach at 510 nm was observed indicating the presence of additional species (**Figure**

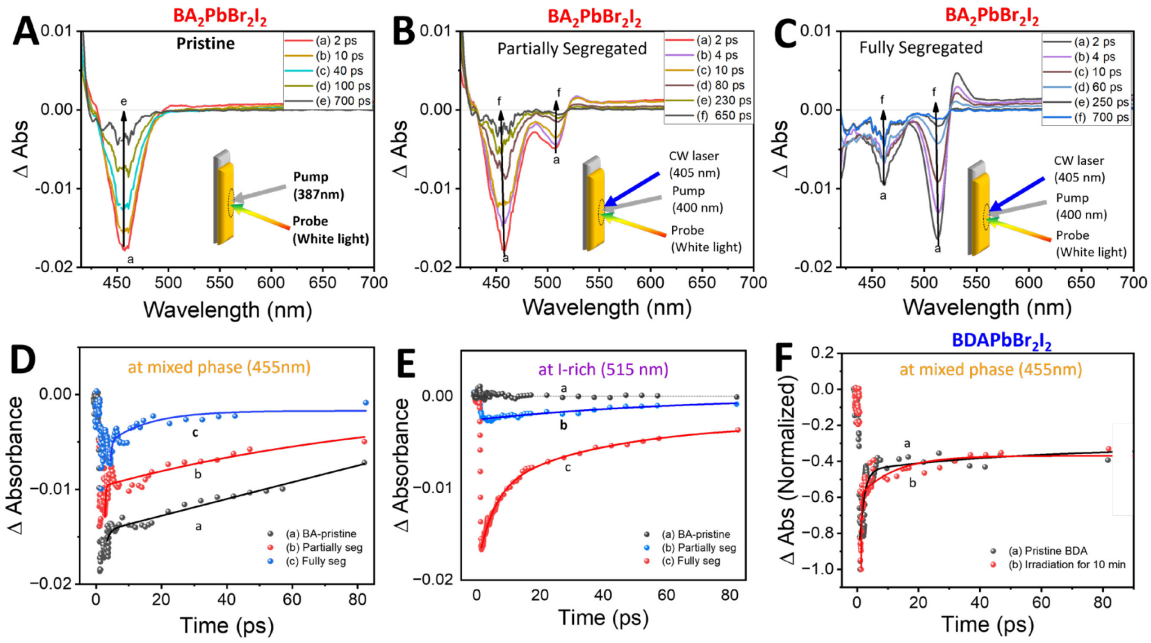

Figure 4. (A-C) Time-resolved difference absorption spectra recorded following 400 nm laser pulse excitation (32 μJ/cm^2) of $BA_2PbBr_2I_2$: (A) pristine, (B) partially segregated (5 min), and (C) fully segregated film (10 min) under CW 405 nm diode laser intensity of 50 mW/cm^2, respectively. (D,E) Bleach recovery kinetics and fitting by tracking the (D) mixed halide phase peak (at 455 nm) and (E) I-rich domain peak (at 515 nm) using pristine, partially segregated, and fully segregated $BA_2PbBr_2I_2$ films as shown in panels A-C. (F) Bleach recovery kinetics and fitting of $BDAPbBr_2I_2$ film before and after irradiation using 405 nm diode laser with light intensity of 50 mW/cm^2 for 10 min.

4B). This absorption bleach further increased in the fully segregated film along with decreased contribution from the parent bleach (**Figures 4C**). The increased population of I-rich domains as part of segregation in mixed halide BA-RP perovskite contributes to the bleach at 510 nm. The progressive response of iodide phase and decrease of parent mixed halide phase with increased continuous light irradiation time further highlights the changing composition and related excited behavior of segregated BA-RP films during halide phase segregation. It should be noted that spectral overlaps between the pump wavelength and Br-rich domain peak (at 400 nm) did not allow probing of Br domain in the halide segregated film and its recovery kinetics.

We followed the excited state deactivation by monitoring the bleach recovery of the mixed halide peak (455 nm) for these BA-RP films with varying degree of segregation. The bleach recovery traces were fitted using biexponential kinetic expression (See **Table S2** for parameters of the kinetic fits). The average lifetimes of bleach recovery were 166 ps (without segregation), 100 ps (partially segregated), and 4.4 ps (fully segregated) (**Figure 4D**). In the case of unsegregated film, exciton and charge carrier recombination dominate the excited state deactivation within the parent mixed halides. On the other hand, in the segregated films the charge carriers from mixed halide perovskite phase are funneled to iodide rich phase, thus accelerating the excited state deactivation. The bleach recovery kinetics at I-rich domain, thus, provide direct evidence of excited state interactions and charge transfer. As anticipated, the pristine film does not exhibit a bleach at I-rich domain (indicative of no segregation), whereas both partially and fully segregated films displayed bleach signals at 515 nm (corresponding to I-rich domain) under a CW 405 nm laser diode irradiation. The bleach recovery kinetics at I-rich domain were determined to be 47 ps (for partially segregated) and 21 ps (for fully segregated). The continuous hole injection for partially segregated films elongated the bleach recovery kinetics whereas the almost I-rich domain at fully segregated film undergoes intrinsic e-h recombination with decreased hole transfer from the mixed halide phase. (**Figure 4E**).

The TA experiments were repeated using BDA-DJ perovskite films while keeping the film irradiated with a CW 405 nm diode laser using same irradiation conditions (**Figures 4F, S9, and Table S3**). It is also important to note that inherently, there is a difference in average lifetime of bleach recovery between BA-RP and BDA-DJ films before halide segregation. The extracted average lifetime was determined to be 166 ps (BA-RP) and 9 ps (BDA-DJ). It is well known that enhanced electronic coupling of inorganic layers along out-of-plane direction with reduced organic spacing distance in DJ perovskites facilitate exciton delocalization across adjacent inorganic layers with reduced quantum confinement.[65] This behavior aligns with the suppressed PL emission intensity observed in the PL measurements for the hybrid RP-DJ films. All films showed a single bleach corresponding to the parent mixed halide exciton band. The bleach recovery traces remained unperturbed as we continued the laser irradiation of the films. These observations agree with the steady-state absorption measurements discussed in the earlier section and indicate the suppression of halide segregation in BDA-DJ perovskite films.

Mechanistic Understanding of Underlying Iodine Explusion. It is obvious from previous discussion that BDA^{2+} spacer cation suppresses the halide migration in BDA-DJ perovskite films. We further probed its role in suppressing halide segregation followed by expulsion in hybrid RP-DJ 2D perovskite films. The RP-DJ films with different BA:BDA compositions were immersed in dichloroethane (DCE) and were subjected to 405 nm continuous irradiation. The expulsion of iodine was quantified by monitoring the formation of I_3^- in solvent. As discussed previously, 2D perovskite film is in contact with DCE solvent, continuous photoirradiation drives sequential iodide oxidation, migration, and ultimately iodide expulsion into DCE.[16,42,67] **Figures 5A,B** show the time-dependent evolution of I_3^- in DCE with distinct absorption band at 295 and 365 nm, as we irradiate BA-RP and BDA-DJ perovskite films. (Note that expelled I_2 from the perovskite film complexes with dissolved iodide ion to form I_3^- in DCE.) Since BDA-DJ perovskite with covalent interlayer linkage are effective in maintaining the mixed halide phase, we observe relatively less expulsion of I_2 into the solution (equation 2). The effect of BDA in decreasing the rate of I_2 expulsion can also be seen in mixed RP-DJ perovskites. Increasing the fraction of DJ perovskites in mixed RP:DJ compositions progressively suppressed the formation of I_3^- species **(Figure S10)**.

The kinetics of iodine expulsion from irradiated perovskite films were analyzed by tracking the formation of I_3^- species in solutions. The absorption changes at 295 nm which represent I_3^-

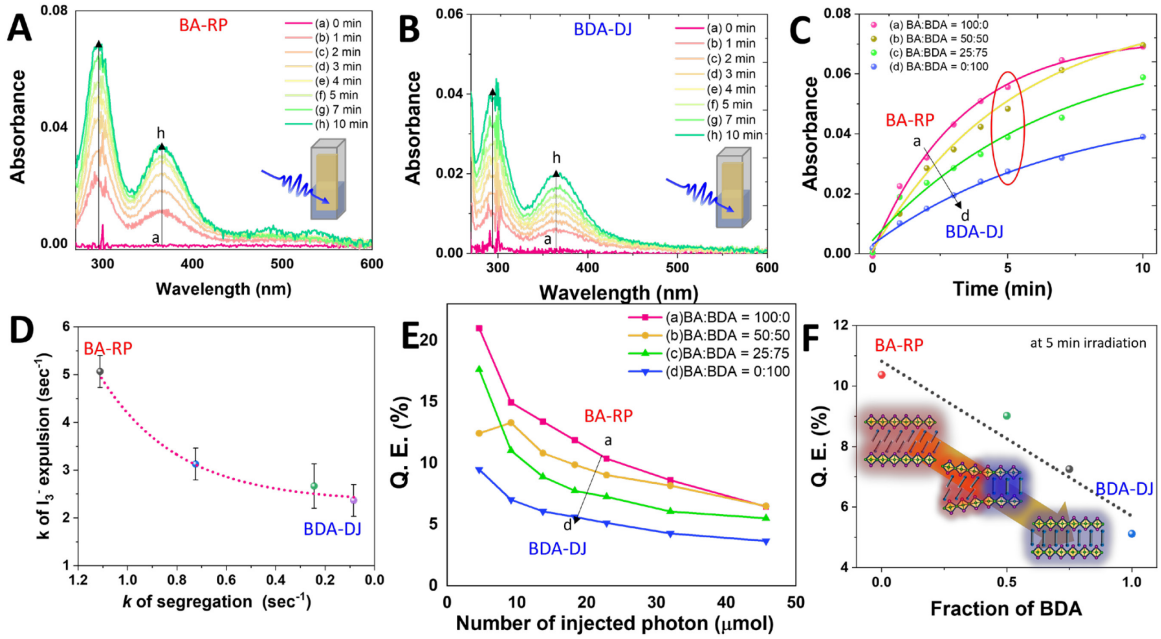

Figure 5. (A,B) Absorption spectra evolution of DCE solution containing (A) $BA_2PbBr_2I_2$ (pure BA 100%) and (B) $BDAPbBr_2I_2$ (pure BDA 100%) film under a CW 405 nm diode laser irradiation (25 mW/cm^2). (C) Kinetic traces and fitting by tracking the 295 nm corresponding to I_3^- with varying BA:BDA ratio from 100:0 – 0:100 (D) Correlation of rate constant of disappearance of mixed halide peak (at 440-450 nm) and that of I_3^- formation. (E) Quantum efficiency of I_3^- generation given injected photon using different mixed RP-DJ perovskite films. (F) Quantum efficiency plot with 5 min photoirradiation with varying the fraction of BDA in mixed BA-BDA phase compositions.

formation, at different irradiation times are plotted in **Figure 5C**. The pseudo-first order rate constants ($k_{expulsion}$) decreased from 5.1 × 10^{-3} sec^{-1} (BA-RP) to 2.3 × 10^{-3} sec^{-1} (BDA-DJ) films. The rigidifying strategy achieved here through bidentate spacer cation is similar to A-site engineering strategy employed in 3D perovskite films (e.g., incorporating inorganic Cs^+ as A-site cations).[23,24,68]

Correlation between kinetic rate constant ($k_{expulsion}$) of I_3^- formation and that of disappearance of mixed halides ($k_{segregation}$) was established in **Figure 5D**. As expected, the I_3^- formation kinetic rate constant decreased exponentially, shifting from BA-RP to BDA-DJ perovskites due to reinforced 2D frameworks with DJ spacers. Quantum efficiency of iodine expulsion during irradiation was calculated using the following equation (4)

$$\text{Q.E. (\%)} = 100 \text{ x } \frac{3\text{nI}_3-}{2n_{photon}} \qquad (4)$$

wherein n_{I3^-} (μmole) is number of I_3^- species generated during photoirradiation and n_{photon} (μmole) is number of photons incident on the perovskite film at a given irradiation time (**Figure S11**). Note that conversion factor of 3/2 was used since one mole of I_3^- corresponds to three iodide species that are expelled following absorption of two photons (equations 2-3).

At a fixed irradiation time, increasing the DJ fraction in the mixed RP-DJ phase compositions led to reduction in iodide expulsion Q.E. due to lower formation of I_3^- species. These reflect that under photoirradiation, the more robust DJ perovskites in which halide segregation does not occur, exhibiting significantly reduced iodide expulsion efficiency (**Figure 5E**). When plotting the Q.E. at 5-minute irradiation *versus* BDA fraction, the Q.E. gradually decreased from 10.4 (BA-RP) to 5.1 % (BDA-DJ) (**Figure 5F**). Therefore, halide segregation and segregated phases can accelerate the iodine expulsion in DCE solvent due to hole accumulation at I-rich domain across the segregated domains.

Based on these observations using steady- and excited-state absorption spectra monitoring the 2D perovskite films or solvent containing I_3^- under continuous photoirradiation, we can propose the halide expulsion mechanism in BDA-DJ and BA-RP perovskite films (**Scheme 2**). Continuous irradiation of mixed halide perovskite films facilitates the halide segregation and subsequent iodide expulsion in BA-RP perovskites due to weaker attachment of RP layer through van der Waals interactions. The segregated halide domain with favorable energetics induces the hole transfer and confinement at I-rich domain. Hole-induced oxidation of iodide (I^-) to monomolecular iodine ($I\cdot$) or bimolecular iodine (I_2) species accelerate dissolution and expulsion of I^- from the 2D lattices in solution with generation of I_3^- species. In contrast, covalently tethered BDA perovskites prevent the octahedral lattice distortion, defection formation, halide ion migration, and segregation under the same photoirradiation.[3,10,69,70] Importantly, the maintenance of mixed halide phase under photoirradiation just induces electron-hole recombination within mixed halide phase, instead.

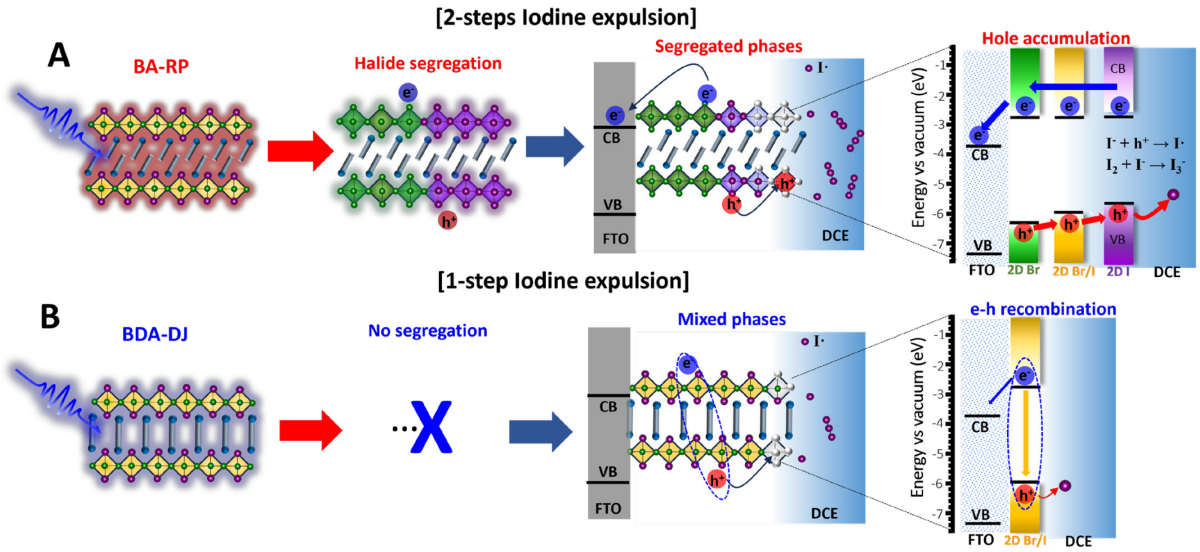

Scheme 2. (A,B) Schematic illustration of photoinduced iodide expulsion including two steps (halide segregation followed by iodide expulsion) and one step (direct iodide expulsion) seen in $BA_2PbBr_2I_2$ (BA 100%; A) and $BDAPbBr_2I_2$ (BDA 100%; B) films, respectively. Corresponding energy diagram of mixed and segregated halides in contact with DCE solution demonstrating the possible excited state charge carrier dynamics.

However, exposure to DCE solvent allow for direct photooxidation of DJ perovskites with iodide expulsion with a significantly reduced kinetics (**Scheme 2**).

In summary, binding configuration of spacer ligands (RP vs DJ) even with the same backbone of the carbon chain (e.g. C_4 in n-butylamine and 1,4-butylenediamine) incorporated into the 2D mixed halide perovskite frameworks govern iodine stability under photoirradiation. Stoichiometric blending of RP-DJ hybrid composition influences the stability of 2D perovskite films. Although the halide segregation is reversible in the dark when irradiated for a short time, extended period of photoirradiation causes expulsion of iodine resulting in irreversible transformations. Through synergetic incorporation of mixed RP-DJ spacers with enhanced structural stability can improve both processability and stability (and water-repellant hydrophobicity), thus allowing for optimizing the performance and stability of perovskite optoelectronics. Recently, phase engineering through blending different 2D phase (RP-DJ) is effective in balancing the performance and stability of optoelectronic devices such as perovskite solar cells and light-emitting diodes.[62,71,72] This strategy can enable synergistically improve the charge carrier dynamics with improved structural integrity through precisely tuning the structural phases. This study offers a significant insight into degradation of halide perovskites through halide ion migration and expulsion as well as strategical methods for developing more stable and efficient 2D/3D perovskite solar cells.

Conflict of Interest

The authors declare no conflict of interest.

Corresponding Author Information

Junsang Cho – School of Energy and Chemistry, Sungshin Women's University, Seoul 01133, South Korea; ORCID https://orcid.org/0000-0003-4211-4113; Email: jcho3@sungshin.ac.kr

Prashant Kamat - Radiation Laboratory, Department of Chemistry and Biochemistry and Department of Chemical and Biomolecular Engineering, University of Notre Dame, Notre Dame, Indiana 46556, United States; ORCID https://orcid.org/0000-0002-2465-6819; Email: pkamat@nd.edu

Acknowledgement

The work is supported by the Division of Materials Sciences and Engineering Office of Basic Energy Sciences of the U.S. Department of Energy through Award DE-SC0014334 to study the ion migration effects in metal halide perovskites. J. Cho acknowledges the support by the National Research Foundation of Korea (NRF) grant funded by the Korea government (MSIT) (NRF-2022R1C1C1004131). This is contribution number NDRL No. 5488 from the Notre Dame Radiation Laboratory

Supporting Information

The Supporting Information is available free of charge at https://xxxx.

Experimental details and additional characterization (UV-vis absorption, PL emission spectra, XPS characterizations, SEM images, Quantum efficiency calculation, and transient absorption spectra).

References

(1) Zhao, Y.; Yavuz, I.; Wang, M.; Weber, M. H.; Xu, M.; Lee, J. H.; Tan, S.; Huang, T.; Meng, D.; Wang, R.; Xue, J.; Lee, S. J.; Bae, S. H.; Zhang, A.; Choi, S. G.; Yin, Y.; Liu, J.; Han, T. H.; Shi, Y.; Ma, H.; Yang, W.; Xing, Q.; Zhou, Y.; Shi, P.; Wang, S.; Zhang, E.; Bian, J.; Pan, X.; Park, N. G.; Lee, J. W.; Yang, Y. Suppressing Ion Migration in Metal Halide Perovskite via Interstitial Doping with a Trace Amount of Multivalent Cations. *Nat. Mater.* **2022**, *21* (12), 1396–1402.

(2) Xu, Z.; Kerner, R. A.; Kronik, L.; Rand, B. P. Beyond Ion Migration in Metal Halide Perovskites: Toward a Broader Photoelectrochemistry Perspective. *ACS Energy Lett.* **2024**, 4645–4654.

(3) Dubose, J. T.; Kamat, P. V. Hole Trapping in Halide Perovskites Induces Phase Segregation. *Accounts Mater. Res.* **2022**, *3* (7), 761–771.

(4) Motti, S. G.; Meggiolaro, D.; Barker, A. J.; Mosconi, E.; Perini, C. A. R.; Ball, J. M.; Gandini, M.; Kim, M.; De Angelis, F.; Petrozza, A. Controlling Competing Photochemical Reactions Stabilizes Perovskite Solar Cells. *Nat. Photonics* **2019**, *13* (8), 532–539.

(5) Kuno, M.; Brennan, M. C. What Exactly Causes Light-Induced Halide Segregation in Mixed-Halide Perovskites? *Matter* **2020**, *2* (1), 21–23.

(6) Elmelund, T.; Seger, B.; Kuno, M.; Kamat, P. V. How Interplay between Photo and Thermal Activation Dictates Halide Ion Segregation in Mixed Halide Perovskites. *ACS Energy Lett.* **2020**, *5* (1), 56–63.

(7) Dubose, J. T.; Kamat, P. V. TiO2-Assisted Halide Ion Segregation in Mixed Halide Perovskite Films. *J. Am. Chem. Soc.* **2020**, *142* (11), 5362–5370.

(8) Yoon, S. J.; Draguta, S.; Manser, J. S.; Sharia, O.; Schneider, W. F.; Kuno, M.; Kamat, P. V. Tracking Iodide and Bromide Ion Segregation in Mixed Halide Lead Perovskites during Photoirradiation. *ACS Energy Lett.* **2016**, *1* (1), 290–296.

(9) Cho, J.; Mathew, P. S.; DuBose, J. T.; Kamat, P. V. Photoinduced Halide Segregation in Ruddlesden–Popper 2D Mixed Halide Perovskite Films. *Adv. Mater.* **2021**, *33* (48), 1–8.

(10) Min, S.; Jeon, M.; Cho, J.; Bang, J. H.; Kamat, P. V. Spectroelectrochemical Insights into the Intrinsic Nature of Lead Halide Perovskites. *Nano Converg.* **2024**, *11* (1), 49.

(11) Xu, Z.; Kerner, R. A.; Harvey, S. P.; Zhu, K.; Berry, J. J.; Rand, B. P. Halogen Redox Shuttle Explains Voltage-Induced Halide Redistribution in Mixed-Halide Perovskite Devices. *ACS Energy Lett.* **2023**, *8* (1), 513–520.

(12) Xu, Z.; Zhong, X.; Hu, T.; Hu, J.; Kahn, A.; Rand, B. P. Correlating Halide Segregation with Photolysis in Mixed-Halide Perovskites via In Situ Opto-Gravimetric Analysis. *J. Am. Chem. Soc.* **2024**, *146* (49), 33368–33377.

(13) Kerner, R. A.; Xu, Z.; Larson, B. W.; Rand, B. P. The Role of Halide Oxidation in Perovskite Halide Phase Separation. *Joule* **2021**, *5* (9), 2273–2295.

(14) Jana, C.; Samu, G. F.; Balog, Á.; De Angelis, F.; Meggiolaro, D.; Kamat, P. V.; Janáky, C. Electrochemical Hole Injection Selectively Expels Iodide from Mixed Halide Perovskite Films. *J. Am. Chem. Soc.* **2019**, *141* (27), 10812–10820.

(15) Choe, H.; Jeon, D.; Lee, S. J.; Cho, J. Mixed or Segregated: Toward Efficient and Stable Mixed Halide Perovskite-Based Devices. *ACS Omega* **2021**, *6* (38), 24304–24315.

(16) Xu, Z.; Kerner, R. A.; Berry, J. J.; Rand, B. P. Iodine Electrochemistry Dictates Voltage-Induced Halide Segregation Thresholds in Mixed-Halide Perovskite Devices. *Adv. Funct. Mater.* **2022**, *32* (33), 2203432.

(17) Quan, L. N.; Yuan, M.; Comin, R.; Voznyy, O.; Beauregard, E. M.; Hoogland, S.; Buin, A.; Kirmani, A. R.; Zhao, K.; Amassian, A.; Kim, D. H.; Sargent, E. H. Ligand-Stabilized Reduced-Dimensionality Perovskites. *J. Am. Chem. Soc.* **2016**, *138* (8), 2649–2655.

(18) Quan, L. N.; Zhao, Y.; García De Arquer, F. P.; Sabatini, R.; Walters, G.; Voznyy, O.; Comin, R.; Li, Y.; Fan, J. Z.; Tan, H.; Pan, J.; Yuan, M.; Bakr, O. M.; Lu, Z.; Kim, D. H.;

Sargent, E. H. Tailoring the Energy Landscape in Quasi-2D Halide Perovskites Enables Efficient Green-Light Emission. *Nano Lett.* **2017**, *17* (6), 3701–3709.

(19) Tan, S.; Shih, M. C.; Lu, Y.; Choi, S. G.; Dong, Y.; Lee, J. W. J. H. J. W.; Yavuz, I.; Larson, B. W.; Park, S. Y.; Kodalle, T.; Zhang, R.; Grotevent, M. J.; Lin, Y. K.; Zhu, H.; Bulović, V.; Sutter-Fella, C. M.; Park, N. G.; Beard, M. C.; Lee, J. W. J. H. J. W.; Zhu, K.; Bawendi, M. G. Spontaneous Formation of Robust Two-Dimensional Perovskite Phases. *Science (80-.).* **2025**, *388* (6747), 639–645.

(20) Mao, L.; Stoumpos, C. C.; Kanatzidis, M. G. Two-Dimensional Hybrid Halide Perovskites: Principles and Promises. *J. Am. Chem. Soc.* **2019**, *141* (3), 1171–1190.

(21) Min, S.; Cho, J. Halide Ion Mobility in Paired 2D Halide Perovskites: Ruddlesden–Popper Versus Dion–Jacobson Phases. *Adv. Opt. Mater.* **2024**, *12* (12), 1–10.

(22) Cho, J.; Kamat, P. V. Photoinduced Phase Segregation in Mixed Halide Perovskites: Thermodynamic and Kinetic Aspects of Cl–Br Segregation. *Adv. Opt. Mater.* **2020**, *2001440*, 1–9.

(23) Mathew, P. S.; Szabó, G.; Kuno, M.; Kamat, P. V. Phase Segregation and Sequential Expulsion of Iodide and Bromide in Photoirradiated Ruddlesden-Popper 2D Perovskite Films. *ACS Energy Lett.* **2022**, *7* (11), 3982–3988.

(24) Mathew, P. S.; Mathew, P. S.; Samu, G. F.; Samu, G. F.; Janáky, C.; Kamat, P. V.; Kamat, P. V.; Kamat, P. V. Iodine (I) Expulsion at Photoirradiated Mixed Halide Perovskite Interface. Should i Stay or Should i Go? *ACS Energy Lett.* **2020**, *5* (6), 1872–1880.

(25) Dučinskas, A.; Jung, M.; Wang, Y. R.; Milić, J. V.; Moia, D.; Grätzel, M.; Maier, J. Mixed Ionic-Electronic Conduction in Ruddlesden-Popper and Dion-Jacobson Layered Hybrid Perovskites with Aromatic Organic Spacers. *J. Mater. Chem. C* **2024**, *12* (22), 7909–7915.

(26) Lin, C.; Tang, Y.; Xu, W.; Kumar, P.; Dou, L. Charge Transfer in 2D Halide Perovskites and 2D/3D Heterostructures. *ACS Energy Lett.* **2024**, *9* (8), 3877–3886.

(27) Zhang, F.; Park, S. Y.; Yao, C.; Lu, H.; Dunfield, S. P.; Xiao, C.; Uličná, S.; Zhao, X.; Hill, L. Du; Chen, X.; Wang, X.; Mundt, L. E.; Stone, K. H.; Schelhas, L. T.; Teeter, G.; Parkin, S.; Ratcliff, E. L.; Loo, Y. L.; Berry, J. J.; Beard, M. C.; Yan, Y.; Larson, B. W.; Zhu, K. Metastable Dion-Jacobson 2D Structure Enables Efficient and Stable Perovskite Solar Cells. *Science (80-.).* **2022**, *375* (6576), 71–76.

(28) Yu, D.; Cao, F.; Liao, J.; Wang, B.; Su, C.; Xing, G. Direct Observation of Photoinduced Carrier Blocking in Mixed-Dimensional 2D/3D Perovskites and the Origin. *Nat. Commun.* **2022**, *13* (1), 1–11.

(29) Vasileiadou, E. S.; Wang, B.; Spanopoulos, I.; Hadar, I.; Navrotsky, A.; Kanatzidis, M. G. Insight on the Stability of Thick Layers in 2D Ruddlesden-Popper and Dion-Jacobson Lead Iodide Perovskites. *J. Am. Chem. Soc.* **2021**, *143* (6), 2523–2536.

(30) Fu, P.; Quintero, M. A.; Vasileiadou, E. S.; Raval, P.; Welton, C.; Kepenekian, M.; Volonakis, G.; Even, J.; Liu, Y.; Malliakas, C.; Yang, Y.; Laing, C.; Dravid, V. P.; Reddy, G. N. M.; Li, C.; Sargent, E. H.; Kanatzidis, M. G. Chemical Behavior and Local Structure of the Ruddlesden-Popper and Dion-Jacobson Alloyed Pb/Sn Bromide 2D Perovskites. *J. Am. Chem. Soc.* **2023**, *145* (29), 15997–16014.

(31) Li, X.; Hoffman, J. M.; Kanatzidis, M. G. The 2D Halide Perovskite Rulebook: How the Spacer Influences Everything from the Structure to Optoelectronic Device Efficiency. *Chem. Rev.* **2021**, *121* (4), 2230–2291.

(32) Chakkamalayath, J.; Hiott, N.; Kamat, P. V. How Stable Is the 2D/3D Interface of Metal Halide Perovskite under Light and Heat? *ACS Energy Lett.* **2023**, *8* (1), 169–171.

(33) Szabó, G.; Kamat, P. V. How Cation Migration across a 2D/3D Interface Dictates Perovskite Solar Cell Efficiency. *ACS Energy Lett.* **2024**, *9* (1), 193–200.

(34) Moral, R. F.; Perini, C. A. R.; Kodalle, T.; Kim, A.; Babbe, F.; Harada, N.; Hajhemati, J.; Schulz, P.; Ginsberg, N. S.; Aloni, S.; Schwartz, C. P.; Correa-Baena, J. P.; Sutter-Fella, C. M. Anion and Cation Migration at 2D/3D Halide Perovskite Interfaces. *ACS Energy Lett.* **2024**, *9* (6), 2703–2716.

(35) Niu, K.; Wang, C.; Zeng, J.; Wang, Z.; Liu, Y.; Wang, L.; Li, C.; Jin, Y. Ion Migration in Lead-Halide Perovskites: Cation Matters. *J. Phys. Chem. Lett.* **2024**, *15* (4), 1006–1018.

(36) Mathew, P. S.; Kamat, P. V. Cation Migration in Physically Paired 2D and 3D Lead Halide Perovskite Films. *Adv. Opt. Mater.* **2024**, *12* (8), 1–9.

(37) Samu, G. F.; Janáky, C.; Kamat, P. V. A Victim of Halide Ion Segregation. How Light Soaking Affects Solar Cell Performance of Mixed Halide Lead Perovskites. *ACS Energy Lett.* **2017**, *2* (8), 1860–1861.

(38) Huang, P.; Kazim, S.; Wang, M.; Ahmad, S. Toward Phase Stability: Dion-Jacobson Layered Perovskite for Solar Cells. *ACS Energy Lett.* **2019**, *4* (12), 2960–2974.

(39) Sajjad Ahmad, Ping Fu, Shuwen Yu, Xiuli Wang, Xin Guo, C. L. Dion-Jacobson Phase 2D Layered Perovskites for Solar Cells with Ultrahigh Stability. *Joule* **2019**, *3* (3), 794–806.

(40) Cao, J.; Duan, C.; Li, Z.; Jin, B.; Li, J.; Wan, L.; Zhao, L.; Dong, B.; Wu, C. Theoretical Selection of 2D Perovskite for Constructing Efficient Heterojunction Solar Cells. *ACS Mater. Lett.* **2023**, *5* (4), 970–978.

(41) Liu, C.; Yang, Y.; Fletcher, J. D.; Liu, A.; Gilley, I. W.; Musgrave, C. B.; Wang, Z.; Zhu, H.; Chen, H.; Reynolds, R. P.; Ding, B.; Ding, Y.; Zhang, X.; Skackauskaite, R.; Wan, H.; Zeng, L.; Bati, A. S. R.; Shibayama, N.; Getautis, V.; Chen, B.; Rakstys, K.; Dyson, P. J.; Kanatzidis, M. G.; Sargent, E. H.; Nazeeruddin, M. K. Cation Interdiffusion Control for 2D/3D Heterostructure Formation and Stabilization in Inorganic Perovskite Solar Modules. *Nat. Energy* **2025**, *10*, 981–990.

(42) Szabo, G.; Kuno, M.; Kamat, P. V. Iodine ' s Wild Ride Leading to Photoinstability. *ACS Energy Lett.* **2025**, *10*, 4378–4385.

(43) Knight, A. J.; Borchert, J.; Oliver, R. D. J.; Patel, J. B.; Radaelli, P. G.; Snaith, H. J.; Johnston, M. B.; Herz, L. M. Halide Segregation in Mixed-Halide Perovskites: Influence of A-Site Cations. *ACS Energy Lett.* **2021**, *6* (2), 799–808.

(44) Yu, H.; Xie, Y.; Zhang, J.; Duan, J.; Chen, X.; Liang, Y.; Wang, K.; Xu, L. Thermal and Humidity Stability of Mixed Spacer Cations 2D Perovskite Solar Cells. *Adv. Sci.* **2021**, *8* (12), 1–10.

(45) Lisanne M. Einhaus, Xiao Zhang, Jeroen P. Korterik, Guido Mul, Johan E. ten Elshof, and A. H. Effects of Combining Dion-Jacobson and Ruddlesden-Popper Spacers on The. *Adv. Opt. Mater.* **2024**, *12*, 2401629.

(46) Gong, J.; Hao, M.; Zhang, Y.; Liu, M.; Zhou, Y. Layered 2D Halide Perovskites beyond the Ruddlesden–Popper Phase: Tailored Interlayer Chemistries for High-Performance Solar Cells. *Angew. Chemie* **2022**, *134* (10).

(47) Li, Z.; Zheng, X.; Xiao, X.; An, Y.; Wang, Y.; Huang, Q.; Li, X.; Cheacharoen, R.; An, Q.; Rong, Y.; Wang, T.; Xu, H. Beyond the Phase Segregation: Probing the Irreversible Phase Reconstruction of Mixed-Halide Perovskites. *Adv. Sci.* **2022**, *9* (5), 1–10.

(48) Hu, J.; Xu, Z.; Murrey, T. L.; Pelczer, I.; Kahn, A.; Schwartz, J.; Rand, B. P. Triiodide Attacks the Organic Cation in Hybrid Lead Halide Perovskites: Mechanism and Suppression. *Adv. Mater.* **2023**, *35* (40), 1–8.

(49) Mauck, C. M.; Tisdale, W. A. Excitons in 2D Organic–Inorganic Halide Perovskites. *Trends Chem.* **2019**, *1* (4), 380–393.

(50) Liu, Y.; Ono, L. K.; Tong, G.; Zhang, H.; Qi, Y. Two-Dimensional Dion-Jacobson Structure Perovskites for Efficient Sky-Blue Light-Emitting Diodes. *ACS Energy Lett.* **2021**, *6* (3), 908–914.

(51) Mathew, P. S.; Dubose, J. T.; Cho, J.; Kamat, P. V.; Dubose, J. T.; Cho, J.; Kamat, P. V. Spacer Cations Dictate Photoinduced Phase Segregation in 2D Mixed Halide Perovskites. *ACS Energy Lett.* **2021**, *6* (7), 2499–2501.

(52) Min, Seonhong; Mukherjee, Manish; Szabó, Gábor; Kamat, Prashant V.;, A.; Cho, J. Design Principles of Spacer Cations for Suppressing Phase Segregation in 2D Halide Perovskites. *Chem. Sci.* **2025**, *16*, 21950–21961.

(53) Leung, T. L.; Ren, Z.; Syed, A. A.; Grisanti, L.; Djurišić, A. B.; Popović, J. Photoinduced Segregation Behavior in 2D Mixed Halide Perovskite: Effects of Light and Heat. *ACS Energy Lett.* **2022**, *7* (10), 3500–3508.

(54) Min, S.; Park, S.; Lee, Y. H.; Kim, D.; Cho, J. Halide Ion Exchange Mechanisms in 2D Ruddlesden-Popper Perovskites : Diffusion- vs Reaction-Limited. *Small* **2025**, *2501817*, 1–

11.

(55) Wang, Y. R.; Senocrate, A.; Mladenović, M.; Dučinskas, A.; Kim, G. Y.; Rothlisberger, U.; Milić, J. V.; Moia, D.; Grätzel, M.; Maier, J. Photo De-Mixing in Dion-Jacobson 2D Mixed Halide Perovskites. *Adv. Energy Mater.* **2022**, *12* (26), 2200768.

(56) Mosconi, E.; Alothman, A. A.; Long, R.; Kaiser, W.; De Angelis, F. Intermolecular Interactions of A-Site Cations Modulate Stability of 2D Metal Halide Perovskites. *ACS Energy Lett.* **2023**, *8* (1), 748–752.

(57) Wang, K.; Lin, Z. Y.; Zhang, Z.; Jin, L.; Ma, K.; Coffey, A. H.; Atapattu, H. R.; Gao, Y.; Park, J. Y.; Wei, Z.; Finkenauer, B. P.; Zhu, C.; Meng, X.; Chowdhury, S. N.; Chen, Z.; Terlier, T.; Do, T. H.; Yao, Y.; Graham, K. R.; Boltasseva, A.; Guo, T. F.; Huang, L.; Gao, H.; Savoie, B. M.; Dou, L. Suppressing Phase Disproportionation in Quasi-2D Perovskite Light-Emitting Diodes. *Nat. Commun.* **2023**, *14* (1), 1–11.

(58) Ruiz-Preciado, M. A.; Kubicki, D. J.; Hofstetter, A.; McGovern, L.; Futscher, M. H.; Ummadisingu, A.; Gershoni-Poranne, R.; Zakeeruddin, S. M.; Ehrler, B.; Emsley, L.; Milić, J. V.; Grätzel, M. Supramolecular Modulation of Hybrid Perovskite Solar Cells via Bifunctional Halogen Bonding Revealed by Two-Dimensional 19F Solid-State NMR Spectroscopy. *J. Am. Chem. Soc.* **2020**, *142* (3), 1645–1654.

(59) Milić, J. V.; Zakeeruddin, S. M.; Grätzel, M.; Milic, J. V. Layered Hybrid Formamidinium Lead Iodide Perovskites: Challenges and Opportunities. *Acc. Chem. Res.* **2021**, *54* (12), 2729–2740.

(60) Toso, S.; Gushchina, I.; Oliver, A. G.; Manna, L.; Kuno, M. Are Mixed-Halide Ruddlesden-Popper Perovskites Really Mixed? *ACS Energy Lett.* **2022**, *7* (12), 4242–4247.

(61) Yadav, A. N.; Min, S.; Choe, H.; Park, J.; Cho, J. Halide Ion Mixing across Colloidal 2D Ruddlesden-Popper Perovskites: Implication of Spacer Ligand on Mixing Kinetics. *Small* **2023**, *20* (2305546).

(62) Li, C. H. A.; Ko, P. K.; Chan, C. C. S.; Sergeev, A.; Chen, D.; Tewari, N.; Wong, K. S.; Halpert, J. E. Mixed Ruddlesden–Popper and Dion–Jacobson Phase Perovskites for Stable and Efficient Blue Perovskite LEDs. *Adv. Funct. Mater.* **2023**, *33* (41), 1–9.

(63) Birkhold, S. T.; Precht, J. T.; Liu, H.; Giridharagopal, R.; Eperon, G. E.; Schmidt-Mende, L.; Li, X.; Ginger, D. S. Interplay of Mobile Ions and Injected Carriers Creates Recombination Centers in Metal Halide Perovskites under Bias. *ACS Energy Lett.* **2018**, *3* (6), 1279–1286.

(64) Frolova, L. A.; Luchkin, S. Y.; Lekina, Y.; Gutsev, L. G.; Tsarev, S. A.; Zhidkov, I. S.; Kurmaev, E. Z.; Shen, Z. X.; Stevenson, K. J.; Aldoshin, S. M.; Troshin, P. A. Reversible Pb2+/Pb0 and I−/I3− Redox Chemistry Drives the Light-Induced Phase Segregation in All-Inorganic Mixed Halide Perovskites. *Adv. Energy Mater.* **2021**, *11* (12), 1–11.

(65) Li, W.; Feng, X.; Guo, K.; Pan, W.; Li, M.; Liu, L.; Song, J.; He, Y.; Wei, H. Prominent

Free Charges Tunneling Through Organic Interlayer of 2D Perovskites. *Adv. Mater.* **2023**, *2211808*, 1–10.

(66) Fu, P.; Liu, Y.; Yu, S.; Yin, H.; Yang, B.; Ahmad, S.; Guo, X.; Li, C. Dion-Jacobson and Ruddlesden-Popper Double-Phase 2D Perovskites for Solar Cells. *Nano Energy* **2021**, *88* (April), 106249.

(67) Tran, H. C. V.; Kim, B.; Kim, H.; Park, S.; Woo, J. Y.; Jeong, S. Unraveling the Role of Triiodides in Halide Precursors for Facile Anion Exchange in Lead Halide Perovskite Nanocrystals. *Chem. Mater.* **2022**, *34* (14), 6402–6407.

(68) Susan, P.; Mathew, P.; Cho, J.; Kamat, P. V. Ramifications of Ion Migration in 2D Lead Halide Perovskites. *ACS Energy Lett.* **2024**, *9* (3), 1103–1114.

(69) Gao, X.; Wu, Y.; Zhang, Y.; Chen, X.; Song, Z.; Zhang, T.; Fang, Q.; Ji, Q.; Ju, M. G.; Wang, J. How the Spacer Influences the Stability of 2D Perovskites? *Small Methods* **2025**, *9* (5), 1–9.

(70) Kamat, P. V.; Kuno, M. Halide Ion Migration in Perovskite Nanocrystals and Nanostructures. *Acc. Chem. Res.* **2021**, *54* (3), 520–531.

(71) Yin, M.; Yao, H.; Zhang, M.; Wu, C.; Qiu, H.; Ding, L.; Hao, F. Mixed Dion-Jacobson and Ruddlesden-Popper Tin Halide Perovskite for Efficient and Stable Quasi-2D Lead-Free Solar Cells. *Chem. Eng. J.* **2025**, *508* (February), 161041.

(72) Lin, C.; Tang, Y.; Nian, Z.; Coffey, A. H.; Wang, Y.; Yang, H.; Wu, P.; Yang, Y.; Joy, S.; Graham, K. R.; Xu, W.; Zhu, C.; Savoie, B. M. Intralayer Bidentate Diammoniums for Stable Two-Dimensional Perovskites. *Nat. Chem.* **2025**.